©Civil-Comp Press, 2012
Proceedings of the Eighth International Conference
on Engineering Computational Technology,
B.H.V. Topping, (Editor),
Civil-Comp Press, Stirlingshire, Scotland

Paper 96

Dynamic Analysis of a Porous Layered Medium under a Load Moving along a Railway Track

K. Chahour[1], G. Lefeuve-Mesgouez[1], A. Mesgouez[1]
A. Bouheraoua[2] and A. Laribi[2]
[1] Faculty of Sciences, University of Avignon et des Pays de Vaucluse
UMR EMMAH, Avignon, France
[2] LAMMOMS laboratory
Mouloud Mammeri University of Tizi-Ouzou, Algeria

Abstract

The dynamic response of a poroviscoelastic layered soil medium subjected to a vertical harmonic rectangular moving load is proposed analytically. The moving excitation is applied either directly over the surface of the ground or over a track model. The track model due to Sheng *et al.* [17] takes into account rail, sleepers, pads and ballast. A parametric study is proposed in order to assess the influence of the various parameters on the dynamic response such as load velocity, frequency, porosity and permeability. A comparison between poroviscoelastic and viscoelastic models is considerd. The amplitude of the displacement response is also given for various values of beam rigidity in both sub- and super- Rayleigh regimes.

Keywords: moving load, layered medium, railway track, wave propagation, Biot's theory, Fourier transform.

1 Introduction

The study of vibrations induced by moving loads is an important area of researches because of the intensity of railway traffic. In this context, two main points are of interest: the model of the ground and the model used for the track. For the first point, many researches have been yielded concerning moving loads and modelling the soil as a viscoelastic medium. Sneddon [1] was among the first to carry out the theoretical analysis in 2D and 3D geometries under a moving point load. Cole and Huth [2] introduced then the Mach number to differentiate the case of high load speeds. The three-dimensional half space subjected to a point load moving with a constant velocity was considered by Eason et al. [3]. Alabi [4] studied vibrations due to a set of concentrated moving vertical forces for low load speeds and due to a moving oblique point load for speeds up to half the Rayleigh wavespeed [5]. Fourier integral transforms, Helmholtz's decomposition and a change of frame are commonly used for the theoretical approach. Krylov [6] focused on the contribution of the Rayleigh wave. Jones et al. [7] studied the case of a moving rectangular load ovelying an elastic half-space. De Barros and Luco [8] investigated the response of a stratified viscoelastic half-space to a moving point load. Both these latter articles demonstrate the possibility of shock formation in the ground.

In all these works, the ground is considered as viscoelastic media. However, the soil is composed of a solid skeleton and pore space filled with fluid. Theodorakopoulos [9] and Niki et al [10] showed that in the case of soft materials, models ignoring the coupling between fluid and solid may lead to errors, especially for high velocities. The importance of the interaction between the fluid component and the solid part of the medium is now generally recognised and poroelastic models have become of main interest. Using Biot's theory, Cai et al. [11] presented a semi-analytical approach for a moving rectangular load of constant amplitude on a poroviscoelastic half-space. A comparison between viscoelastic and poroviscoelastic models shows that for higher load speeds, the poroviscoelastic soil displacements are larger than that of the viscoelastic soil whereas they are similar for low load speeds [11]. Lefeuve-Mesgouez et al. [13] proposed a three-dimensional semi-analytical analysis of the vertical displacements induced by a rectangular high-speed moving harmonic load over a totally or partially saturated poroviscoelastic half-pace. Results show that solid displacements are affected by the effect of the soil saturation.Xu et al. [12] presented a semi-analytical approach for a similar configuration but on a layered poroelastic half-space. They use the Transmission and Reflection Matrix method.

The second point of investigation concerns the model used for the railway track. It may be represented by a simple continuous model using an Euler viscoelastic beam. Dieterman and Metrikine [14] studied the equivalent stiffness of a half-space interacting with a beam using a two-dimensional model. In the absence of damping, the stiffness becomes zero at the Rayleigh wavespeed. Lefeuve-Mesgouez et al. [15] showed differences in the amplitude and distribution of solid displacements and fluid pressure of a poroviscoelatic layered half-space when the track is implemented on the ground. Xu et al. [16] show that for the Euler beam overlying a layered poroelastic half-space, there still exist critical velocities even when the load speed is larger than the shear wavespeed.

Sheng et al. [17] proposed a more accurate track model composed of a rails, rail pads and sleepers supported by the ballast. The rails are modelled as an Euler beam. The sleepers are represented as a distributed mass. The rail pads are modelled as a distributed vertical spring between the rail beam and the sleeper mass. The ballast is modelled as a viscoelastic layer with uniformally distributed mass. The ground is modelled as viscoelastic layers overlying either a half-space or a rigid foundation. This model is a reference for numerous works. Indeed, it deals with both constant and harmonic loads. Considering the train-track system composed of rails, sleepers and ballast, Takemiya [18] and Takemiya et al. [19] studied the dynamic responses of a track-ground system on a layered elastic soil. Based on Sheng's model, Picoux et al. [20] developed a three-dimensional semi-analytical model for the response of the ground surface due to vibrations generated by a railway traffic for low vibration frequencies (in the 5-80 Hz range). Cai et al. [21] coupled Sheng's analytical model for the track to a poroviscoelastic half-space. Results for the case of a moving point load [22] show that dynamic responses of the track-ground system are considerably affected by the rail rigidity and also by the load speed. Xia et al. [23] presented a theoretical model of a train-track-soil dynamic interaction for moving-train induced ground vibration. The model consists of a train submodel, a track submodel and a subsoil submodel which are coupled through dynamic interactions of wheel-rail and sleeper-soil, respectively and Green's functions of the subsoil.

In the works coupling the railway track to the ground, except those of Cai et al., Lefeuve-Mesgouez et al. and Xu et al., the soil was considered as an elastic or a viscoelastic medium. However, as there is underground water in the considered soil medium, which affects the wave propagation, the poroelastic soil model is more appropriate than the viscoelastic one. Studies combining a more realistic track system with poroelastic multilayered soil are rather limited.

In this paper, based on the dynamic poroelastic theory of Biot, a semi-analytical approach is used to investigate the vertical dynamic response of a poroviscoelastic stratified ground. The soil is coupled to a track model and subjected to a vertical rectangular harmonic moving load. The railway track is based on Sheng's model which takes into account rail, sleepers, pads and ballast. The implementation of the beam over the ground allows to get the effect of the track on the dynamic response. Thus, soil vertical displacements are numerically evaluated for various values of load speed, porosity and permeability to assess the influence of those parameters on the response of the poroviscoelastic soil. Comparison between poroviscoelastic and viscoelastic models is also proposed.

2 Model Description

2.1 Geometry

The geometry under study is presented on Figure 1. The track model is based on Sheng's model overlying a layer resting on a rigid half-space. The railway is infinite in length and is aligned with respect to the x direction. The contact width with the ground is denoted $2L_{Bal}$. Parameters of the model are presented in section (2.3).

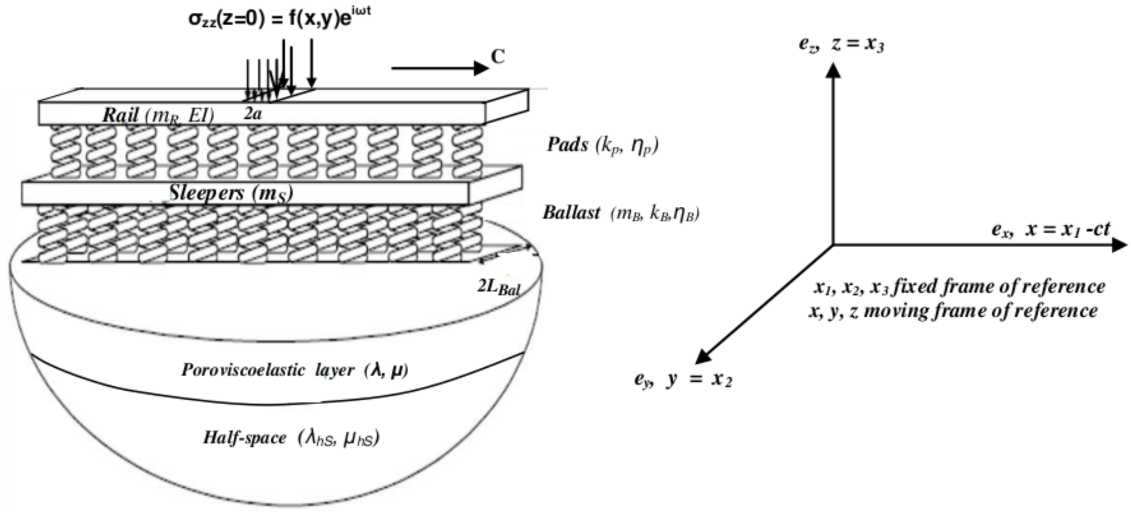

Figure 1: Railway track model.

2.2 Governing equations

In the poro(visco)elastic medium, based on the constitutive equations and the conservation of momentum, we obtain for each homogeneous and isotropic layer

$$\begin{cases} \sigma = (\lambda_0 \, \nabla.\mathbf{u} - \beta \, p) \, \mathbf{I} + 2 \, \mu \, \varepsilon, \\ p = -m \, (\beta \, \nabla.\mathbf{u} + \nabla.\mathbf{w}) \, , \\ \nabla \, \sigma = \rho \, \ddot{\mathbf{u}} + \rho_f \, \ddot{\mathbf{w}}, \\ -\nabla \, p = \rho_f \, \ddot{\mathbf{u}} + \dfrac{a_\infty \, \rho_f}{\phi} \, \ddot{\mathbf{w}} + \dfrac{\eta}{\kappa} \, \dot{\mathbf{w}}, \end{cases} \tag{1}$$

where $\mathbf{u} =< u_{x_1}, \, u_{x_2}, \, u_{x_3} >^t$ is the solid displacement vector, $\mathbf{U} =< U_{x_1}, \, U_{x_2}, \, U_{x_3} >^t$ is the fluid displacement vector, $\mathbf{w} = \phi \, (\mathbf{U} - \mathbf{u}) =< w_{x_1}, \, w_{x_2}, \, w_{x_3} >^t$ is the relative displacement vector. $\mathbf{I}$ is the identity tensor, σ is the stress tensor, $\varepsilon = \frac{1}{2} \, (\nabla \, \mathbf{u} + \nabla^t \, \mathbf{u})$ is the linearised strain tensor, and p is the pore pressure. The physical parameters are : the dynamic viscosity η and the density ρ_f of the saturating fluid; the density ρ_s and the shear modulus μ of the elastic skeleton; the connected porosity ϕ, the tortuosity a_∞, the absolute permeability κ, the Lamé coefficient of the dry matrix λ_0, and the two Biot coefficients β and m of the isotropic matrix. The dots and double dots denote respectively first and second time derivatives.

2.3 Track equations

The model used for the track was first presented by Sheng et al. [17] and is composed of the rail, the sleepers and the ballast. First, the rail is modelled as an infinite Euler viscoelastic beam, for which the cross-section is supposed to be infinitely rigid, as follows

$$EIw_R(x_1,t)_{,x_1x_1x_1x_1} + m_R\ddot{w}_R(x_1,t) + k_P[w_R(x_1,t) - w_S(x_1,t)] = Q(x_1,t) \quad (2)$$

where w_R and w_S are the deflections (i.e. vertical displacements) of the rail and the sleeper respectively, EI the bending rigidity of the rail, m_R the mass per unit of length of the rail. k_P represents the spring constant per unit of length of the pads between the rail and the sleeper.

Q is the applied moving load. For a load distributed over a non-zero width, $Q(x_1,t) = \frac{-Q_0\exp(i\omega t)}{2a}$ if $\mid x \mid = \mid x_1 - ct \mid < a$.

The sleepers can be modelled using the concept of continuous mass: vertical displacements generated by a moving load are almost identical when taking into account a discrete or uniformly distributed distribution of sleepers, see Vostroukhov et al. [24]. Consequently, for the sleepers, the model is written as follows

$$m_S\ddot{w}_S(x_1,t) + k_P[w_S(x_1,t) - w_R(x_1,t)] = F_S(x_1,t) \quad (3)$$

where F_S stands for the sleeper vertical force per unit of length acting on the ballast, and m_S the mass per unit of length of the sleeper.

To finish, at the top and the bottom of the ballast, from Suiker et al. [25], the following equations are written

$$m_B/6[2\ddot{w}_S(x_1,t) + \ddot{w}_B(x_1,t) + k_B[w_S(x_1,t) - w_B(x_1,t)] = -F_S(x_1,t) \quad (4)$$
$$m_B/6[\ddot{w}_S(x_1,t) + 2\ddot{w}_B(x_1,t) + k_B[-w_S(x_1,t) + w_B(x_1,t)] = F_B(x_1,t) \quad (5)$$

where F_B represents the vertical force per unit of length exerted by the ballast on the soil and w_B the vertical displacement of the ballast. k_B and m_B are the spring constant per unit of length and the mass per unit of length of the ballast. Dampings in pads and ballast are taken into account using a modified hysteretic damping with constants η_P and η_B.

2.4 Interface conditions

The interface conditions between the ballast and the ground, for $x_3 = 0$, are written as follows:

$$\sigma_{33}(x_1,x_2,x_3=0) = \frac{-F_B}{2L_{bal}} \text{ if } \mid x_2 \mid < L_{bal} \quad (6)$$
$$\sigma_{13}(x_1,x_2,x_3=0) = 0 \qquad \sigma_{23}(x_1,x_2,x_3=0) = 0 \quad (7)$$
$$p(x_1,x_2,x_3=0) = 0 \quad (8)$$
$$u_3(x_1,x_2,x_3=0) = w_B(x_1) \quad (9)$$

3 Semi-analytical solution

Pressure and stress components are eliminated from Eqs. (1), giving a $(\mathbf{u},\ \mathbf{w})$ second-order wave formulation

$$\begin{cases} (\lambda_0 + \mu + m\,\beta^2)\,\nabla(\nabla.\mathbf{u}) + \mu\,\nabla^2\,\mathbf{u} + m\,\beta\,\nabla(\nabla.\mathbf{w}) = \rho\,\ddot{\mathbf{u}} + \rho_f\,\ddot{\mathbf{w}}, \\ m\,\beta\,\nabla(\nabla.\mathbf{u}) + m\,\nabla(\nabla.\mathbf{w}) = \rho_f\,\ddot{\mathbf{u}} + \dfrac{a\,\rho_f}{\phi}\ddot{\mathbf{w}} + \dfrac{\eta}{\kappa}\,\dot{\mathbf{w}}. \end{cases} \tag{10}$$

The solid and relative displacements in Eqs. (10) can be expressed by

$$\mathbf{u} = \nabla\,\varphi + \nabla\ \times \boldsymbol{\Psi}, \qquad \mathbf{w} = \nabla\,\varphi^r + \nabla\ \times \boldsymbol{\Psi}^r, \tag{11}$$

where φ and φ^r are scalar potentials, and $\boldsymbol{\Psi}$ and $\boldsymbol{\Psi}^r$ are vector potentials.
We then introduce the moving frame of reference defined as $x = x_1 - ct,\ y = x_2,\ z = x_3$ and use Fourier transforms over space variables x and y, defined as follows

$$g(x,\ y) = \int_{-\infty}^{+\infty} \overline{\overline{g}}(k_x,\ k_y) exp(ik_x x) exp(ik_y y) dk_x dk_y \tag{12}$$

$$\overline{\overline{g}}(k_x, k_y) = \frac{1}{4\pi^2}\int_{-\infty}^{+\infty} g(x,\ y)\exp(-ik_x x)\exp(-ik_y y) dx dy \tag{13}$$

Mass, stiffness and damping matrices are introduced as follows

$$[K_P] = \begin{bmatrix} \lambda_0 + 2\mu + m\beta^2 & M\beta \\ m\beta & m \end{bmatrix} \quad [K_S] = \begin{bmatrix} \mu & 0 \\ 0 & 0 \end{bmatrix}$$
$$[M] = \begin{bmatrix} (1-\phi)\rho_s + \phi\rho_f & \rho_f \\ \rho_f & \frac{a_\infty \rho_f}{\phi} \end{bmatrix} \quad [C] = \begin{bmatrix} 0 & 0 \\ 0 & \frac{\eta}{\kappa} \end{bmatrix}$$

Applying the double Fourier transform and considering a harmonic load, decoupled ordinary differential systems are obtained in the wavenumber domain, (14) and (15), relative respectively to compressionnal waves P_1 and P_2 (Helmholtz scalar potentials φ and φ^r) and shear wave S (Helmholtz vector potentials Ψ and Ψ^r), see [13].

$$\left(-\left(\frac{d^2}{dz^2} - k_x^2 - k_y^2\right)[K_P] - (\omega - k_x c)^2[M] + i(\omega - k_x c)[C]\right)\left\{\begin{array}{c} \overline{\overline{\varphi}}^* \\ \overline{\overline{\varphi}}^{r*} \end{array}\right\} = \left\{\begin{array}{c} 0 \\ 0 \end{array}\right\} \tag{14}$$

$$\left(-\left(\frac{d^2}{dz^2} - k_x^2 - k_y^2\right)[K_S] - (\omega - k_x c)^2[M] + i(\omega - k_x c)[C]\right)\left\{\begin{array}{c} \overline{\overline{\Psi}}^* \\ \overline{\overline{\Psi}}^{r*} \end{array}\right\} = \left\{\begin{array}{c} \mathbf{0} \\ \mathbf{0} \end{array}\right\} \tag{15}$$

The star exponent denotes the amplitude of the function considered: $\overline{\overline{\varphi}}(k_x, k_y, \omega) = \overline{\overline{\varphi}}^*(k_x, k_y)\exp(i\omega t)$. Vertical components k_{zPj} of the compressional wavenumber vectors $\mathbf{k}_{Pj}$ are obtained from the dispersion relation (16).

$$\det\left[(k_x^2 + k_y^2 + k_{zPj}^2)[K_P] - (\omega - k_x c)^2[M] + i(\omega - k_x c)[C]\right] = 0,\ j = 1, 2 \tag{16}$$

with $j=1$, for the P_1 wave and $j=2$ for the P_2 wave, $k_{Pj}^2 = k_x^2 + k_y^2 + k_{zPj}^2$.
Similarly, vertical component k_{zS} of the shear wavenumber vector $\mathbf{k}_S$ is obtained

$$k_{zS}^2 = -k_x^2 - k_y^2 + \frac{(\omega - k_x c)^2}{\mu}\left([(1-\phi)\rho_s + \phi\rho_f] + \rho_f\, G(\omega, k_x, k_y)\right) \tag{17}$$

with $k_S^2 = k_x^2 + k_y^2 + k_{zS}^2$.
The exact stiffness matrix approach is based on vectors of transformed displacement and stress components, see [26], defined as $\overline{\overline{\mathbf{u}}}^* = < \overline{\overline{u}}_x^*, \overline{\overline{u}}_y^*, i\overline{\overline{u}}_z^*, i\overline{\overline{w}}_z^* >^t$ and $\overline{\overline{\mathbf{\Sigma}}}^* = < \overline{\overline{\sigma}}_{xz}^*, \overline{\overline{\sigma}}_{yz}^*, i\overline{\overline{\sigma}}_{zz}^*, -i\overline{\overline{p}}^* >^t$. Analytical expression for the vector of transformed displacements is then given by the solution of the matrix system, see [15]

$$\underbrace{\begin{bmatrix} \mathrm{S}^T & \mathrm{S}^R\mathrm{Z}(h_n) \\ -\mathrm{S}^T\mathrm{Z}(h_n) & -\mathrm{S}^R \end{bmatrix}\begin{bmatrix} \mathrm{Q}^T & \mathrm{Q}^R\mathrm{Z}(h_n) \\ \mathrm{Q}^T\mathrm{Z}(h_n) & \mathrm{Q}^R \end{bmatrix}^{-1}}_{\mathbf{T}^n_{(8\times 8)}} \begin{Bmatrix} \overline{\overline{\mathbf{u}}}^*(z=z_{n-1}) \\ \overline{\overline{\mathbf{u}}}^*(z=z_n) \end{Bmatrix} = \begin{Bmatrix} \overline{\overline{\Sigma}}^*(z=z_{n-1}) \\ -\overline{\overline{\Sigma}}^*(z=z_n) \end{Bmatrix} \tag{18}$$

where $\mathrm{Q}^{T/R}$, $\mathrm{S}^{T/R}$ and $\mathrm{Z}(h_n)$ are 4×4 matrices, h_n denotes the n^{th} layer's depth. The superscripts T and R stand for transmitted and reflected waves respectively. In the case of the half-space (*hs*), only the transmitted terms are kept and $\mathrm{T}^{hs} = \mathrm{S}^T(\mathrm{Q}^T)^{-1}$. Then a classical assembling technique between the porous layers uses the continuity of stresses and displacements at each interface. The resulting matrix system has dimension $4(N+1)\times 4(N+1)$ for a three-dimensional problem, with N the number of different layers. In the resulting vector $\overline{\overline{\mathbf{\Sigma}}}^*$, all terms equal zero, except $\overline{\overline{\sigma}}_{zz}(z=0)$ that is linked to the track using the interface condition.

Considering the track equations (2, 3, 4 and 5), they are modified firstly by the change of variables, secondly by the Fourier transform but only on the x space variable, and thirdly by the elimination of $\overline{F_S}^*(k_x,\omega)$. Consequently, the rail-sleeper-ballast system behavior is governed by 3 equations as follows

$$A_1(k_x,\omega)\overline{w_R}^*(k_x,\omega) - k_P\overline{w_S}^*(k_x,\omega) = A_2(k_x) \tag{19}$$
$$k_P\overline{w_R}^*(k_x,\omega) + A_3(k_x,\omega)\overline{w_S}^*(k_x,\omega) + A_4(k_x,\omega)\overline{w_B}^*(k_x,\omega) = 0 \tag{20}$$
$$A_4(k_x,\omega)\overline{w_S}^*(k_x,\omega) + A_5(k_x,\omega)\overline{w_B}^*(k_x,\omega) = -\overline{F_B}^*(k_x,\omega) \tag{21}$$

with

$$\begin{aligned}
A_1(k_x,\omega) &= EIk_x^4 - m_R(\omega - k_x c)^2 + k_P \\
A_2(k_x) &= \overline{Q}^*(k_x) \\
A_3(k_x,\omega) &= m_S(\omega - k_x c)^2 + m_B/3(\omega - k_x c)^2 - k_P - k_B \\
A_4(k_x,\omega) &= m_B/6(\omega - k_x c)^2 + k_B \\
A_5(k_x,\omega) &= m_B/3(\omega - k_x c)^2 - k_B
\end{aligned}$$

where $\overline{Q}^*(k_x) = -Q_0\frac{sin(ak_x)}{ak_x}$ for a load distributed over a non-zero width.

In the previous system, $(\overline{w_R}^*, \overline{w_S}^*, \overline{w_B})^*$ and $\overline{F_B}^*$ are unknowns. To obtain $\overline{F_B}^*$, another equation is thus needed. It is obtained with the interface condition between the ballast and the ground (6):

$$\overline{\overline{\sigma_{zz|z=0}}}(k_x, k_y, \omega)^* = -\overline{F_B}^*(k_x, \omega)\frac{sin(k_y L_{bal})}{k_y L_{bal}} \tag{22}$$

Moreover, the Fourier transform of displacement continuity between the ballast and the ground (9), written along the mean line ($y = 0, z = 0$), can be expressed as follows

$$\left[\frac{1}{2\pi}\int_{-\infty}^{+\infty} \overline{w_B}^*(k_x, \omega)\exp(ik_x x)dk_x\right]_{z=0} =$$
$$\left[\frac{1}{4\pi^2}\int_{-\infty}^{+\infty}\int_{-\infty}^{+\infty} \overline{\overline{u_z}}^*(k_x, k_y, \omega)^*\exp(ik_x x)\exp(ik_y y)dk_y dk_x\right]_{y=z=0}$$

from which it comes

$$[\overline{w_B}^*(k_x, \omega)]_{z=0} = \left[\frac{1}{2\pi}\int_{-\infty}^{+\infty} \overline{\overline{u_z}}^*(k_x, k_y, \omega)dk_y\right]_{z=0} \tag{23}$$

Noting $\overline{\overline{u}}^*|^{\circledcirc}_{z=0}$ the transformed vertical solid displacement for a unit vertical harmonic stress $\overline{\overline{\sigma}}^*_{zz}|_{z=0} = 1$, such as $[T]\{\overline{\overline{u}}^*|^{\circledcirc}_{z=0}\} =< 0, 0, i, 0, ..., 0 >^t$, one gets

$$\overline{\overline{u_z}}^*|_{z=0} = \overline{\overline{u}}^*|^{\circledcirc}_{z=0}\ \overline{\overline{\sigma_{zz|z=0}}}^* = -\overline{\overline{u}}^*|^{\circledcirc}_{z=0}\overline{F_B}^*(k_x, \omega)\frac{sin(k_y L_{bal})}{k_y L_{bal}} \tag{24}$$

Consequently, combining relations (22), (23) and (24), the coupling of the ballast and the ground gives

$$\overline{w_B}^*(k_x, \omega) = -\left(\frac{1}{2\pi}\int_{-\infty}^{+\infty}\overline{\overline{u}}^*|^{\circledcirc}_{z=0}(k_x, k_y, \omega)\frac{sin(k_y L_{bal})}{k_y L_{bal}}dk_y\right)\overline{F_B}^*(k_x, \omega) \tag{25}$$

$$\overline{w_B}^*(k_x, \omega) = -A_6(k_x, \omega)\overline{F_B}^*(k_x, \omega) \tag{26}$$

$A_6(k_x, \omega)$ is obtained using a Gauss-Legendre quadrature technique. Physically speaking, A_6 represents the flexibility of the poroviscoelastic soil subjected to the force applied by the ballast (and therefore the track structure) in the transformed domain. As the integrand is an even function, one can write

$$A_6(k_x, \omega) = \frac{1}{\pi}\int_0^{+\infty}\overline{\overline{u}}^*|^{\circledcirc}_{z=0}(k_x, k_y, \omega)\frac{sin(k_y L_{bal})}{k_y L_{bal}}dk_y$$

Thus we get four unknowns ($\overline{w_R}^*, \overline{w_S}^*, \overline{w_B}^*$ and $\overline{F_B}^*$) for four equations (19, 20, 21, 25). From this system, it is of interest to get the expression for $\overline{F}^*_B$ as follows

$$\overline{F_B}^*(k_x, \omega) = \frac{-k_P A_2 A_4}{A_1 A_4^2 A_6 + (1 - A_5 A_6)(A_1 A_3 + k_P^2)} \tag{27}$$

Once $\overline{F_B}^*(k_x, \omega)$ has been determined, the stresses are determined with (22) and included in the poroviscoelastic multilayered formulation of the ground (18) to address the solid and relative displacements in the soil. From system (19-21), deflection of the rail, sleeper or ballast can also be deduced.

4 Parametric study

4.1 Case of a soil directly subjected to a rectangular load

The first case under consideration concerns a poroviscoelastic layer resting on a rigid half-space with λ_{hs} = 2.33×10^{11} Pa, μ_{hs} = 10^{11} Pa. The system is considered without track. The applied load is rectangular with dimensions $2a \times 2b$ = 0.3×0.3 m. The layer's depth is H = 18 m. A double Fast Fourier Transform (FFT) algorithm is used to perform the inverse transform with respect to k_x and k_y. To compute the inverse transform accurately with a discrete transform, the integrals must be truncated at sufficiently high values to avoid aliasing, while the mesh of the calculated functions must be fine enough to represent well details of the functions. To satisfy these requirements, we used 2048×2048 points and $|k_x, k_y| < 120$ m^{-1} for a frequency f = 64 Hz, for instance.
Parameters of the saturated poroelastic half-space are selected refer to Theodorakopoulos [9]: λ_0 = 2.33×10^8 Pa, μ = 10^8 Pa, $\rho_s = 1816$ kg/m^3, ρ_f = 1000 kg/m^3, ϕ = 0.4, β = 1, m = 5.56 GPa and a_∞ = 1.
Corresponding Rayleigh, shear, first compressional and second compressional wave speeds are given by : v_R = 243 m.s^{-1}, v_S = 260 m.s^{-1}, v_{P1} = 19 m.s^{-1} and v_{P2} = 2006 m.s^{-1}, respectively.

4.1.1 Influence of porosity

As it is known in Biot's theory, porosity is one of the governing parameters of a porous medium. It is thus of interest to study the effect of this physical parameter on the displacements of a poroviscoelastic soil. Figures 2 and 3 show the normalized maximum vertical soil displacements varied with load speed for various values of porosity and for two values of hydraulic permeability K where $K = \frac{k}{\eta}$. The displacement is normalized with respect to the displacement response calculated for zero load speed which are similar in each case. In addition, the load speed c is normalized with respect to shear wavespped c_S which is given by 247 m/s and 260 m/s for ϕ = 0.2 and 0.4, respectively. Two values of frequency are considered, f = 1 Hz and f = 64 Hz corresponding to the quasi-static and the dynamic regime, respectively.

As shown in figures 2 and 3, all the curves are similar, specifically for the case a fine soil (K = 10^{-9}m^{3}s/kg) and f = 1 Hz for which all the curves reach a maximum at about c = $0.93 v_s$ (figure 2 b). This peak corresponds to a load velocity near the Rayleigh-wave velocity (c_R = 243 m/s). For this value of permeability and for the dynamic regime (f = 64 Hz), lower amplitude of the response is given by a lower value of porosity when it corresponds to a higher value of porosity for a more permeable soil (K = 10^{-7}m^{3}s/kg) and for f = 1 Hz (figure 3 (b)).
Two peaks appear in the case of a dynamic regime for a fine material (K = 10^{-9}m^{3}s/kg). The first peak corresponds to value of the load speed around the Rayleigh-wave speed. From figure 3 (a), values of the normalized displacements are similar for the dynamic

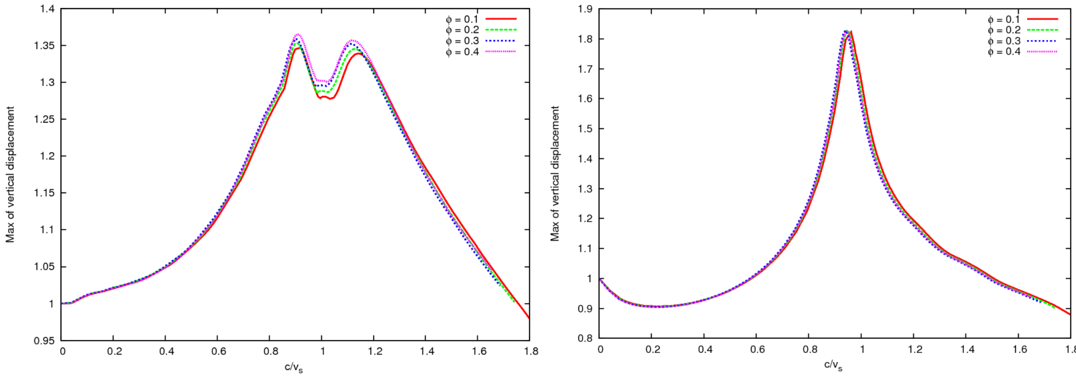

(a) (b)

Figure 2: Variation of the normalised maximun soil vertical displacement versus load speed for various values of porosity, $K = 10^{-9}$m^{3}s/kg: (a) $f = 64$ Hz, (b) $f = 1$ Hz.

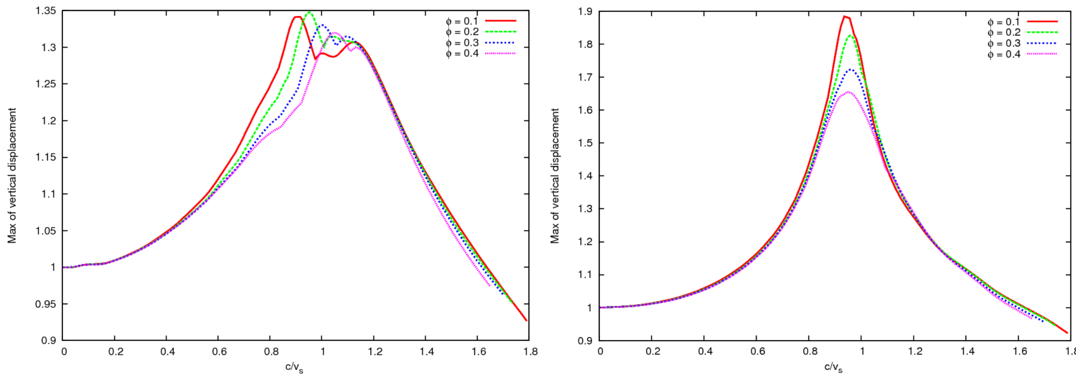

(a) (b)

Figure 3: Variation of the normalised maximun soil vertical displacement versus load speed for various values of porosity, $K = 10^{-7}$m^{3}s/kg: (a) $f = 64$ Hz, (b) $f = 1$ Hz.

regime, until $c/v_s = 0.45$. For a coarse material ($K = 10^{-7}$m^{3}s/kg) and in the case of a quasi-static regime, figure 3 (b) shows a gap between peaks of the curves. For the dynamic regime, the gap occurs before the peak.
Finally, figures 2 and 3 reveal that for both the coarse and the fine soils, the effect of porosity on displacement response is limited only for values of velocity near the Rayleigh wavespeed and no change is observed with change of porosity even for high values of load velocity. This was also seen by Theodorakopoulos [9], in the 2D case and for a constant amplitude.

4.1.2 Influence of permeability

This section concerns the influence of permeability on the displacement response. Figure 4 presents the variation of the normalized maximum soil displacements versus load speed for various kinds of soils and for $f = 64$ Hz and $f = 1$ Hz. For the sake of

comparison, displacements response of a viscoelastic medium is also presented. Two kinds of viscoelastic continuum are studied, both having values for λ_0 and μ given in section (4.1). For the first one, denoted as viscoelastic 1, ρ_s = 1816 Kg/m^3 and for the second one, denoted as viscoelastic 2, ρ_s = 1490 Kg/m^3 issued from the expression : $\rho = (1-\phi)\rho_s + \phi\rho_f$.
Values of the maximum vertical solid displacements u$_{sz}^{max}$ corresponding to zero load speed c = 0, for f = 64 HZ are 1.00×10^{-05} m for K = 10^{-9}m^{3}s/kg, 1.16×10^{-05} m for K = 10^{-7}m^{3}s/kg and 1.19×10^{-05} m for the two viscoelastic soils. For f = 1 Hz, values of u$_{sz}^{max}$ are 1.25×10^{-05} m for K = 10^{-9}m^{3}s/kg and 1.30×10^{-05} m for K = 10^{-7}m^{3}s/kg. Values of the shear wavespeed v_S are equal to 235 m/s, 259 m/s and 260 m/s, for viscoelastic 1, viscoelastic 2 and poroviscoelastic soils, respectively.

In the dynamic regime, except the curve corresponding to a more permeable soil (K = 10^{-7}m^{3}s/kg) which presents one peak, two peaks occur in all the others. The first one is given for a value of c = $0.93 v_S$ and corresponds to the Rayleigh wave velocity. In the quasi-static regime (f = 1 Hz), all the curves are similar and present a peak for values of the load velocity near the Rayleigh wavespeed. Otherwise, the surface displacement response of the viscoelastic ground is higher than the poroviscoelastic one. This phenomenon was also seen by Theodorakopoulos [9] and for a constant amplitude. Indeed, no difference is shown between curves corresponding to viscoelastic soils.
It is also clear from the previous figure that the normalized displacements decrease with decreasing permeability, in the quasi-static regime (f = 1 Hz), except for values of the load speed near the Rayleigh wavespeed for which displacements are higher for a lower permeability (K = 10^{-9}m^{3}s/kg). This may be due to the reduced capacity of the fluid to undertake part of the applied load.

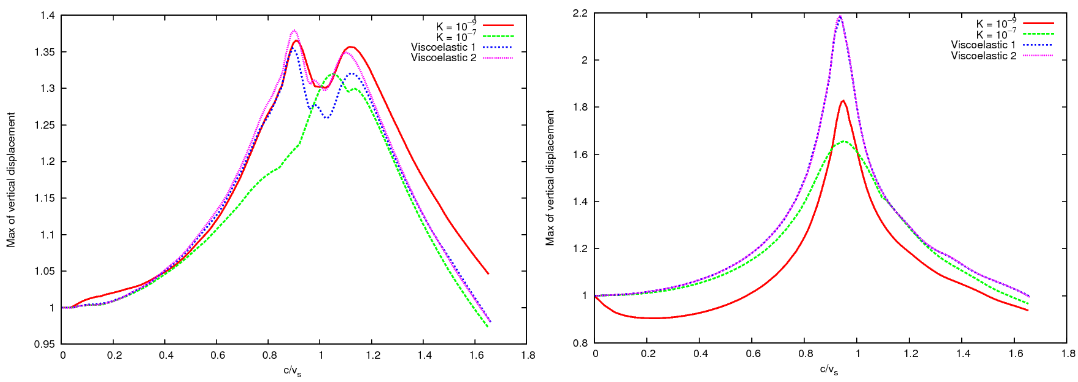

(a) (b)

Figure 4: Variation of the normalised maximun soil vertical displacement versus speed load for various values of permeability: f = 64 Hz, (b) f = 1 Hz.

4.2 Case of a soil incorporating the Sheng's model

Consider now, the case of a poroviscoelastic soil with introducing a railway track (see figure 1). Soil dynamic responses are investigated for a frequency load $f = 64$ Hz. Dimensions of the rectangular applied load are $2a \times 2b = 0.3 \times 1.6$ m. The load width corresponds to the ballast width. With parameters used here, an FFT algorithm with 4096×4096 points and a range of $|k_x, k_y| < 40$ m^{-1} is used.
Parameters for the track are those used by Picoux et al. [20] : $E = 2.11 \times 10^{11}$ N.m^{-2}, $I = 3055$ cm^4, $m_R = 60.34$ kg.m^{-1}, $m_s = 191$ kg.m^{-1}, $k_p = 60 \times 10^6$ N.m^{-2}, $\eta_p = 0.2$, $m_B = 1200$ kg.m^{-1}, $k_B = 3.15 \times 10^8$ N.m^2, $\eta_B = 1$ and $2L_{bal} = 1.6$ m.

4.2.1 Influence of permeability

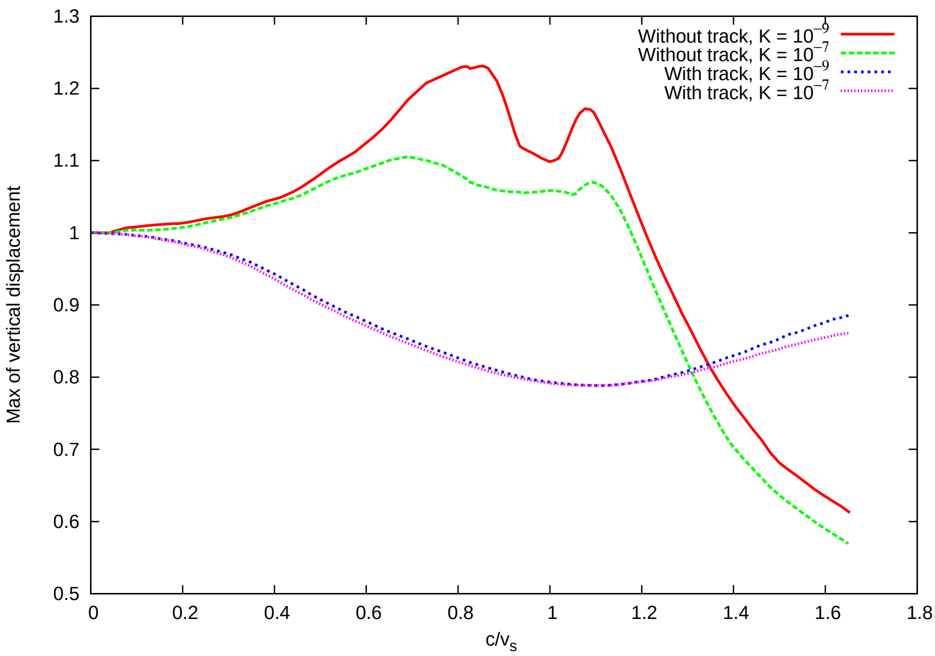

Figure 5: Amplitude of the normalized maximum vertical solid displacement with/without track for various values of permeability: $f = 64$ Hz.

Figure 5 compares the normalized maximum soil displacements versus load velocity, for various values of permeability. Values of the maximum vertical solid displacements u_{sz}^{max} corresponding to zero load speed $c = 0$ in the case of a soil with a track, are: 0.97×10^{-06} m and 1.01×10^{-06} m for $K = 10^{-9}$m^{3}s/kg and $K = 10^{-7}$m^{3}s/kg, respectively. In the case of a soil without track, u_{sz}^{max} is given by 3.24×10^{-06} m and 3.71×10^{-06} m for $K = 10^{-9}$m^{3}s/kg and $K = 10^{-7}$m^{3}s/kg, respectively. The effect of the beam on the soil displacement response is important and the amplitude is obviously reduced when taking into account the presence of a track. In this case, the response curves present the same trends for any value of permeability, even for high load velocity. Indeed, in this case, curves present a minimum for a correspondig velocity to $c = 1.1v_S = 286$ m/s which corresponds to the range of a super-Rayleigh regime. When the track is omitted, the effect of permeability is more noticeable and the displacements become higher for a low permeability. This phenomenon was also observed in the case of a load with dimensions $2a \times 2b = 0.3 \times 0.3$ m (see section 4.1.2). For a low permeability, the first peak occurs for a load speed near the Rayleigh wavespeed ($c = 0.9v_S$).

4.2.2 Effect of beam rigidity

The track rigidity is an important factor and it has an obvious effect on the rail fatigue and the rail service life. The effect of rail rigidity on the vertical soil displacements are shown in figure 6, with a frequency load $f = 64$ Hz.

Whether the load is moving in both the sub- and super-Rayleigh regimes, soil displacement decreases prominently with increasing the beam's stiffness. Moreover, they are more important for $M_R = 0.5$, except for the case of a stiffer beam where the amplitude of vertical displacements remains approximately equal for both regimes. Nevertheless, the amplitude is higher behind the load in the case of a super- Rayleigh regime. A second peak appears for $M_R = 1.5$ beyond $x > 0$, in the case of a softer beam which corresponds to the critical beam speed. In the case of a stiffer beam, both critical velocities approach each other and further emerge, resulting in one critical resonance speed. This was also seen by Suiker et al. [27] in the case of a beam coupled to a half-plane. The authors noted that the number of critical states can arise, depending on the beam's stiffness.

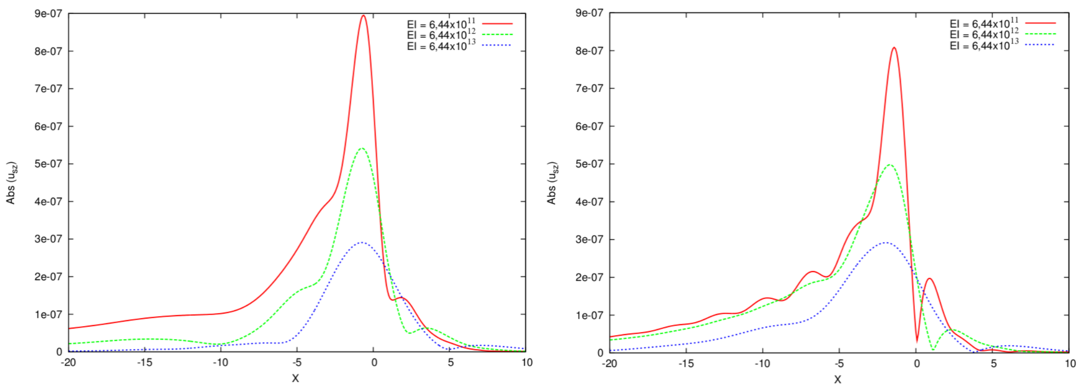

(a) (b)

Figure 6: Effect of beam rigidity on the soil vertical displacement: (a) $M_R = 0.5$, (b) $M_R = 1.5$.

5 Conclusion

Based on the dynamic poroelastic theory of Biot, a semi-analytical approach has been presented in this paper, to study the dynamic response of a poroviscoelastic layered ground induced by a vertical harmonic rectangular moving load. The moving excitation is applied either directly over the soil surface or over the Sheng's track model. The track model which takes into account rail, sleepers, pads and ballast was coupled to a poroviscoelastic layer resting on a rigid half-space. However, the bresults have shown effects and relative importance of the numerous parameters involved, such as porosity, permeability, frequency and speed of the moving load. A comparison between viscoelastic and poroviscoelastic models has been also proposed. The implementation of the track allowed to get the effect of beam on the dynamic vertical response. Numerical results have been presented in the spatial domain for sub- and super- Rayleigh regimes, when varying stiffness of the beam. Nevertheless, for further studies, it is of interest to take into account the influence of other parameters such as the mass of the railway track components on both the deflection of the soil and the track. The applied load may be also considered with other geometries.

References

[1] Sneddon I. 'The stress produced by a pulse of pressure moving along the surface of a semi-infinite solid'. Rendiconti del Circulo Matematico di Palermo, Vol 1 (2), 57-62, 1952.

[2] Cole J, Huth J. 'Stresses produced in a half plane by moving load'. J Appl Mech, 433-36, 1958.

[3] Eason G, Fulton J, Sneddon IN. 'Generation of waves in an infinite elastic solid by variable body forces'. Phil Trans Roy Soc A 248, 575-607, 1956.

[4] Alabi B. 'A model for the problem of ground vibration induced by the wheels of a moving train'. App Math Modeling, 13, 710-15, 1989.

[5] Alabi B. 'A parametric study on some aspects of ground-borne vibrations due to rail traffic'. J Sound Vib 153, 71-87, 1992.

[6] Krylov VV. 'Generation of ground vibrations by superfast trains'. Appl Acoust 44, 149-64, 1995.

[7] Jones DV, Le Houédec D, Peplow AT, Petyt M. 'Ground vibration in the vicinity of a moving harmonic rectangular load on a half-space'. Eur J Mech, A/Solids 17 (1), 153-66, 1998.

[8] De Barros FCP, Luco JE. 'Response of a layered visco-elastic half space to a moving point load'. Wave Motion, 19, 189-210, 1994.

[9] Theodorakopoulos DD. 'Dynamic analysis of a poroelastic half-plane soil medium under moving loads'. Soil Dyn Earthq Eng 23, 521-33, 2003.

[10] Niki ND, Theodorakopoulos DD. 'Dynamic effects of moving loads on road pavements: A review'. Soil Dyn Earthq Eng 31, 547-67, 2011.

[11] Cai Y, Sun H, Xu C. 'Steady state responses of poroelastic half-space soil medium to a moving rectangular load'. Int J Solids Struct 44, 7183-96, 2007.
[12] Xu B, Lu JF, Wang JH. 'Dynamic response of a layered water-saturated half-space to a moving load'. Comput Geotech 35, 1-10, 2008.
[13] Lefeuve-Mesgouez G, Mesgouez A. 'Vibration in the vicinity of a high-speed moving harmonic strip load'. Int J Sol Struct 45 (11-12), 3353-74, 2008.
[14] Dieterman HA, Metrikine AV. 'The equivalent stiffness of a half space interacting with a beam. Critical velocities of a moving load along the beam'. Eur J Mech 15 (1), 67-90, 1996.
[15] Lefeuve-Mesgouez G, Mesgouez A. 'Three-dimensional dynamic response of a porous multilayered ground under moving loads of various distributions'. Adv Eng Software 46, 75-84, 2012.
[16] Xu B, Lu JF, Wang JH. 'Dynamic response of an infinite beam overlying a poroelastic half space to moving loads'. J Sound Vib 306, 91-110, 2007.
[17] Sheng X, Jones CJC, Petyt M. 'Ground vibration generated by a harmonic load acting on a railway track'. J Sound vib 225 (1), 3-28, 1999.
[18] Takemiya H. 'Simulation of trackground vibrations due to a high-speed train: the case of X-2000 at Ledsgard'. J Sound Vib 261, 503-26, 2003.
[19] Takemiya H, Bian XC. 'Substructure simulation of inhomogeneous track and layered ground dynamic interaction under train passage'. J Eng Mech 131, 699-711, 2005.
[20] Picoux B, Le Houédec D. 'Diagnostic and prediction of vibration from railway trains'. Soil Dyn Earthq Eng 25, 905-21, 2005.
[21] Cai Y, Sun H, Xu C. 'Response of railway track system on poroelastic half-space soil medium subjected to moving train load'. Int J Sol Struct 45, 5015-34, 2008.
[22] Cai Y, Sun H, Xu C. 'Three-dimensional simulation of track on poroelastic half-space vibrations due to a moving point load'. Soil Dyn Earthq Eng 30, 958-67, 2010.
[23] Xia H, Cao YM, De Roeck G. 'Theoretical modeling and characteristic analysis of moving-train induced ground vibrations'. J Sound Vib 329, 819-32, 2010.
[24] Vostroukhov AV, Metrikine AV. 'Periodically supported beam on a visco-elastic layer as a model for dynamic analysis of a high-speed railway track'. Int J Sol Struct 40 (21), 5723-52, 2003.
[25] Suiker ASJ, Chang C, De Borst R, Esveld C, 'Surface waves in a stratified half space with enhanced continuum properties. Part 2 : analysis of the wave characteristics in regard to high speed railway tracks'. Eur J Mech A/Sol 18, 769-87, 1999.
[26] Degrande G, De Roeck G, Van Den Broeck P, Smeulders D. 'Wave propagation in layered dry, saturated and unsaturated poroelastic media'. Int J Sol Struct 35 (34-35), 4753-78, 1998.
[27] Suiker ASJ, De Borst R, Esveld C, 'Critical behaviour of a Timoshenko beam-half plane system under a moving load'. Arch of Appl Mech 68, 158-68, 1998.